Impact of EfOM in the elimination of PPCPs by UV/chlorine: Radical chemistry and toxicity bioassays

Yuru Wang, Mauricius Marques dos Santos, Xinxin Ding, Jérôme Labanowski, Bertrand Gombert, Shane Allen Snyder, Jean-Philippe Croué

Version of Record: https://www.sciencedirect.com/science/article/pii/S0043135421008290
Manuscript_e58873dee0a896c2072d9218820c1501

Impact of EfOM in the Elimination of PPCPs by UV/chlorine: Radical chemistry and toxicity bioassays

Yuru Wang[a,b]*, Mauricius Marques dos Santos[c], Xinxin Ding[a], Jérôme Labanowski[b], Bertrand Gombert [b], Shane Allen Snyder[c], Jean-Philippe Croué[b]*

[a] Department of Environmental Science, School of Geography and Tourism, Shaanxi Normal University, Xi'an 710119, China

[b] Institut de Chimie des Milieux et des Matériaux IC2MP UMR 7285 CNRS, Université de Poitiers, France

[c] Nanyang Environment & Water Research Institute (NEWRI), Nanyang Technological University, 1 Cleantech Loop, CleanTech One, #06-08, 637141, Singapore

* Corresponding author
E-mail address: wangyuru@snnu.edu.cn; jean.philippe.croue@univ-poitiers.fr

Abstract: The UV/chlorine process as a potential tertiary municipal wastewater treatment alternative for removing refractory PPCPs has been widely investigated. However, the role of effluent organic matter (EfOM) on the radical chemistry and toxicity alteration is unclear. The elimination of two model PPCPs, primidone (PRM) and caffeine (CAF), by the co-exposure of UV and free chlorine was investigated to elucidate the impact of EfOM. Experimental results indicated that both •OH and reactive chlorine species (RCS) were importantly involved in the decay of PRM at acidic condition, while ClO• played dominant role at alkaline pH. The decay of CAF was dominated by ClO• under all conditions. Chlorine dose, initial contaminant concentration, solution pH, and water matrix affect the process efficiency at varying degree resulting from their specific effect on the radical speciation in the system.

Presence of EfOM isolate remarkably inhibited the decay of PRM and CAF by preferentially scavenging RCS and particularly $ClO^{\bullet}$. Good correlations (linear for PRM and exponential for CAF) between UV absorbance at 254 nm and the observed pseudo first-order rate constants (k'_{obs}) for all EfOM solutions were obtained, demonstrating the importance of aromatic moieties in inhibiting the degradation of targeted contaminants by UV/chlorine process. Degradation of PRM/CAF in reconstituted effluent spiked with the major effluent constituents (i.e., EfOM isolates, Cl^-, HCO_3^-, and NO_3^-) was comparable to the results obtained with the real WWTP effluent and fit well to the correlation between k'_{obs} and UV absorbance at 254 nm, suggesting that EfOM isolates can be used to determine the efficiency of UV/chlorine process in real effluent. EfOM serves as the main precursors of adsorbable organic chlorine in the UV/chlorine treatment. Bioassays indicated that chlorine-containing compounds could induce oxidative stress, mitochondrial dysfunction, and increase the cell DNA damage. Among evaluated treatment conditions, the nature of EfOM, hydrophobic versus transphilic fraction, is likely the predominant factor affecting the cytotoxicity. Meanwhile the UV/chlorine treatment can significantly reduce the cytotoxicity of the EfOM isolates. However, adding high level of selected contaminants (e.g., PRM and CAF) can inhibit this phenomenon due to competition with reactive radicals.

Key words: Effluent organic matter, Primidone, Caffeine, Reactive chlorine species, Adsorbable organic chlorine

1. Introduction

The increasing occurrence of pharmaceutical and personal care products (PPCPs) in environmental matrix has raised great public concerns. These complex compounds are frequently detected at ng L^{-1} to μg L^{-1} concentration levels in varied aquatic environments (Yang et al., 2017). The presence of PPCPs induces potential threat to aquatic organisms and human health (Hamid et al., 2021). Many PPCPs cannot be effectively eliminated by conventional wastewater treatment processes, leading to their continuous discharge into the environment (Yang et al., 2017). It is of great importance to develop and incorporate advanced techniques to efficiently remove PPCPs from WWTPs effluent before their discharge.

Recently, the UV/chlorine process has emerged as a promising alternative for PPCP removal. UV irradiation of free chlorine (FC, HOCl/OCl^-) can generate non-selective hydroxyl radical ($^{\bullet}OH$) and selective reactive chlorine species (RCS, e.g., $Cl^{\bullet}$, $Cl_2^{\bullet-}$, and $ClO^{\bullet}$), leading to the elimination of PPCPs resistant to both UV photolysis and chlorination (Guo et al., 2017). Compared to H_2O_2 and persulfate, chlorine species have relative higher molar absorbance coefficients (i.e., HClO: 59 M^{-1} cm^{-1}; ClO^-: 66 M^{-1} cm^{-1}) and higher quantum yields (>1.0 M E^{-1} s^{-1}) at UV_{254} wavelength (Feng et al., 2007; Watts and Linden, 2007), leading to a higher radical production. Particularly, the simultaneous generation of diverse and more or less selective radical species with high redox potentials (E_0 = 1.8-2.7, 2.4, and 2.0 V for $^{\bullet}OH$, $Cl^{\bullet}$, and $Cl_2^{\bullet-}$, respectively (Buxton et al., 1988; Beitz et al., 1998) provides the

UV/chlorine process complementary reactivities toward a broad spectrum of molecular structures. $Cl^{\bullet}$ preferentially reacts with organic compounds bearing electron-rich moieties at comparable or higher reaction rate constants compared to $^{\bullet}OH$, while $Cl_2^{\bullet-}$ exhibits considerable reactivity toward olefinic compounds and molecules containing phenol, alkoxy benzene, and aniline groups (Lei et al., 2019). Additionally, recent studies have demonstrated the predominant role of $ClO^{\bullet}$ (1.5-1.8 V) in degrading specific PPCPs, such as trimethoprim, carbamazepine, and caffeine with high rate constants ranging from 10^8-10^{10} M^{-1} s^{-1} (Guo et al., 2018).

However, effluent organic matter (EfOM) contained in WWTP effluent is of significant concern for the application of UV/chlorine process in practical conditions. EfOM is a major component of effluent matrix and occurs at concentration (mg L^{-1}) several orders of magnitude higher than that of micropollutants (ng L^{-1}) (Crittenden et al., 2005). EfOM is generally recognized as a heterogenous mixture of non-biodegradable dissolved organic matter (DOM) derived from drinking water, trace levels of refractory organic micropollutants (e.g., PPCPs), and soluble microbial products (O'Connor et al., 2019). The presence of EfOM remarkably impacts the radical chemistry of UV/chlorine process by scavenging radical species, consuming FC, and inducing UV light attenuation via the inner filter effect. Our recent study observed that EfOM isolate exerted a much stronger inhibition on the UV/chlorine process compared with surface water DOM fractions possibly due to its higher abundance in sulfur-containing functional groups (i.e., sink of $^{\bullet}OH/Cl^{\bullet}$ radicals) (Wang et al., 2020). The scavenging effect of EfOM on $ClO^{\bullet}$ is even more pronounced,

thereby significantly reducing degradation kinetics of PPCPs dominated by $ClO^{\bullet}$ oxidation (Guo et al., 2017). Formation of chlorinated byproducts (e.g., DBPs) and the associated toxicity is another important issue of concern. EfOM enriched in nitrogenous moieties serves as a major source of precursors for a wide range of DBPs (Krasner et al., 2009; Le Roux et al., 2017). Compared to chlorination, the UV/chlorine process alters the organic matter through synergistic mechanisms of UV photolysis, chlorination, and reactive radical species. $Cl^{\bullet}/Cl_2^{\bullet-}$ can induce the formation of chlorinated byproducts via direct addition to DOM/EfOM, meanwhile RCS also enhances the yield of high molecular weight nitrogen-containing DBPs (Bulman and Remucal, 2020). Increased formation of adsorbable organic halogen (AOX) and cytotoxicity was observed in UV/chlorine treatment of DOM compared with that of chlorination alone (Wang et al., 2017). Therefore, it is of great importance to assess the impact of EfOM on the efficacy and toxicity of UV/chlorine process for PPCPs removal. Past studies mainly focused on the occurrence of regulated or known DBPs from UV/chlorine treatment of a specific contaminant or DOM fraction and individual toxicity assay. The vast majority of unidentified chlorinated byproducts as indicated by analysis of AOX (i.e., a collective parameter of halogenated DBPs) and their contribution to toxicity remain unclear.

Herein, this study aimed to reveal the impact of EfOM on the radical chemistry and toxicity alteration of UV/chlorine process for PPCPs removal. Primidone (PRM) and caffeine (CAF) were selected as the model PPCPs due to their wide occurrence in aquatic environment and well elucidated radical mechanisms in UV/chlorine process

under varying water scenarios which allow the comparison with our study (Sun et al., 2016; Guo et al., 2018; Wang et al., 2020). Experiments in ultrapure water, real WWTP effluent, and reconstituted effluent spiked with contaminants were conducted to elucidate the key factors affecting the treatment efficiency. Adsorbable organic chlorine (AOCl) analysis in conjunction with multiple *in vitro* bioassays on HepG2 cells were conducted to comprehensively evaluate the formation and cytotoxicity of chlorinated byproducts under complex EfOM matrix.

2. Materials and methods

2.1 Chemicals and materials

All chemicals were of analytical-reagent grade or higher and used as received. The details of chemical sources and stock solutions are provided in Text S1 in the Supplementary Information (SI).

A secondary wastewater effluent sample was collected from a municipal WWTP in Xi'an, China and used for the EfOM isolation and real wastewater effluent test. A XAD-8®/XAD-4® resin adsorption chromatography protocol applied by Drewes and Croué (2002) was employed in this study to adsorb and isolate the organic matter present in the secondary wastewater effluent after reducing pH to 2 and prefiltering with 0.45 μm. Accordingly, two EfOM fractions were obtained, i.e., the hydrophobic (HPO) EfOM fraction retained by XAD-8® resin and transphilic (TPI) EfOM fraction adsorbed by the XAD-4® resin. Adsorbed organics were eluted from the XAD resins by the acetonitrile/water desorption method and then lyophilized to get the solid EfOM fraction (i.e., EfOM isolate).

2.2 Experimental procedures

Experiments were conducted under magnetic stirring and temperature control (23 ± 2 °C) in a UV apparatus equipped with six 8 W low-pressure UV lamps emitting at 254 nm above the petri dish (inner diameter = 95 mm, volume = 250 mL) containing reaction solution (Figure S1). The average UV fluence rate entering the solution was determined as 1.04 $mW \cdot cm^{-2}$ using the iodide/iodate chemical actinometry (Bolton et al., 2011).

For kinetic experiments, a 100 mL phosphate buffer solution (PBS, 5 mM) containing 5 µM PRM or CAF was exposed to UV irradiation in the presence of 70 µM (i.e., 5 mg L^{-1}) FC for 10 min. The UV lamp was warmed up at least 30 min prior to the experiments. Samples (1 mL) were withdrawn at given time intervals and quenched by slight stoichiometry excess of $Na_2S_2O_3$ before HPLC analysis. Experiments with higher concentrations of contaminant (50 µM) and FC (200 µM) were conducted to identify the byproducts during PRM and CAF degradation by the UV/chlorine process and sample preparation is detailed in Text S2.

AOCl formation and toxicity experiments were conducted with a 200 mL solution of 5 µM micropollutant and 70 µM FC buffered at pH 7 with 5 mM PBS in the presence or absence of EfOM isolate (5 mg-C L^{-1}). After 10 min UV exposure, residual chlorine was quenched with slight stoichiometry excess of $Na_2S_2O_3$ which was selected as quenching agent rather than sodium sulfite to minimize the interference for subsequent analysis (Croué and Reckhow, 1989; Ina et al., 2014). Dark chlorination experiments in amber bottles with headspace-free were conducted

following the same procedure. For toxicity assay, 4 identical experiments were conducted in a row, thereby 800 mL sample was obtained and subjected to solid phase extraction (SPE, see Text S2 for the extraction procedure) using a Bond Elut-PPL cartridge (1 g, 6 mL, Agilent). The cartridge was then eluted with 10 mL methanol of LC-MS grade and the eluate was blow-dried with a gentle stream of nitrogen. DMSO of 200 μL was added to the eluate as a keeper and served as the final reconstitution solvent (Dabrowski, 2016).

2.3 Analytical methods

PRM, CAF, and nitrobenzene (NB) were quantified by a Dionex UltiMate 3000 HPLC system. Tentative identification of PRM and CAF transformation byproducts following UV/chlorine treatment was conducted by high resolution LC-MS (Orbitrap Q-Exactive, Thermo Scientific, USA) and GC-MS (GC-QTOF, Agilent, USA). The presence of selected contaminants in the EfOM isolates was quantified by LC-MS/MS (Shimadzu 8060 LC-MS equipped with an electrospray ionization source). AOCl was determined by an adsorption/pyrolysis/microcoulometric analytical method using an Analytik Jena multiX 2500 AOX/TOX analyser equipped with an APU 28 adsorption module. The detailed HPLC, high resolution LC-MS and GC-MS, LC-MS/MS, and AOCl analysis methods are provided in SI Text S3. Chlorine concentration was determined by the DPD method (Moore et al., 1984). The specific UV absorbance (SUVA) for EfOM isolate was calculated as the ratio of the UV absorption coefficient (cm^{-1}) at λ = 254 nm to the concentration of total organic carbon in solution (Vario TOC analyzer, Elementar Analysensysteme GmbH, Germany).

182 **2.4 Kinetic modeling simulation**

183 A previously developed and validated kinetic model using Kintecus, version
184 V6.70 (Ianni, 2018) was updated and modified based on current experimental
185 conditions to evaluate the steady-state concentrations of reactive radicals (Wang et al.,
186 2020). The rate constants of reactions involved in the UV/chlorine process for the
187 modelling were provided in Table S1. The validation of the current model was further
188 verified through the comparison of experimental data vs. model prediction (Table S2)

189 **2.5 Toxicity bioassays**

190 Cell-based assays were selected to evaluate cytotoxicity, induction of cellular
191 reactive oxygen species, DNA damage, and mitochondrial dysfunction. Selection
192 criteria is further discussed under section 3.6.

193 **Cell Culture:** HepG2 cells were purchased from the American Type Culture
194 Collection (ATCC HB-8065); cells were cultured in Dulbecco's Modified Eagle
195 Medium (DMEM) with 10% fetal bovine serum (FBS) at 37°C and 5% carbon
196 dioxide atmosphere.

197 **Cytotoxicity, reactive oxygen species (ROS), and DNA damage:** A colorimetric
198 method (MTS assay; Cell Aqueous, Promega) was used for determining cell viability
199 (i.e., cytotoxicity). A fluorogenic probe (CellROX Green Reagent, Invitrogen) was
200 used for oxidative stress detection. For DNA damage detection, a phosphorylation of
201 histone H2AX (pH2AX) detection kit was used according to manufacturer
202 instructions (HCS DAN Damage Kit, Invitrogen). In a 96 well plate, 40,000 cells
203 were seeded into each plate well with 100 µL of phenol red free DMEM/2%FBS and

incubated for 16 hours. Cell culture media was replaced with fresh media and wells were treated for 24 hours with either SPE extracts or assay controls (n=5) to a final DMSO concentration of 1% DMSO for cytotoxicity (equivalent to an enrichment factor of 40X) and 0.5% DMSO for ROS and DNA damage (equivalent to an enrichment factor of 20X). Details of the three test methods are given in Text S4. Results are presented as signal fold change (ROS and DNA damage) over negative control (0.5% DMSO) and % increase (cytotoxicity).

Mitochondrial function: Oxygen consumption rate (OCR) and extracellular acidification rate of live cells were measured using Seahorse XFe96 Analyzer (Agilent Technologies), mitochondrial function measurements were obtained using the Agilent Seahorse XF Cell Mito Stress Test Kit using different modulators of the electron transport chain. Basal respiration, ATP-linked respiration, maximal and reserve capacities, and non-mitochondrial respiration were monitored. Assay conditions used followed manufacturer instruction, 40,000 cells were used in each experimental well, modulators concentration selected were oligomycin 1.0 µM, FCCP 1.0 µM, and rotenone + antimycin A 0.5 µM. A seeding time of 24 hours was used. For acute experiments 8 measurements cycles were used (120 min) and for long term experiments a 24 hours exposure time was used. An enrichment factor of 20X was used (maximum of 0.5% DMSO). All experiments were done in five replicates.

3. Results and discussion

3.1 Kinetics of PRM and CAF degradation in buffered ultrapure water

Both PRM and CAF are characterized as resistant to UV irradiation and direct

oxidation by FC or H_2O_2 (Guo et al., 2018; Miklos et al., 2019). Control experiments confirmed their negligible role in PRM and CAF degradation (< 7%, Figure 1). In contrast, significant enhancement in contaminant elimination (84% for PRM and 99% for CAF in 10 min) was obtained in the UV/chlorine process due to the generation of reactive radical species, meanwhile UV irradiation led to approximately 43% of FC consumption in the system. The loss of PRM by UV/chlorine followed pseudo first-order kinetics (Figure S2). However, the loss of CAF deviated from first-order kinetics and accelerated with reaction progress as observed by previous studies (Sun et al., 2016; Cheng et al., 2018). These differences might be associated with the highly selective characteristic of RCS whose reactivity toward aromatic PPCPs strongly depends on the nature of substituents on aromatic ring and the core structures (Guo et al., 2017). The electron-donating 1-methylimidazole moiety in CAF induced its high reactivity with $ClO^{\bullet}$ related reactive species, which was claimed as the reason for its unique kinetics (Sun et al., 2016). It was reported that $ClO^{\bullet}$ played a major role rather than $^{\bullet}OH$ and $Cl^{\bullet}$ in degrading CAF, while contribution of $^{\bullet}OH$ to the decay of PRM bearing an electron-withdrawing amide group was more substantial compared with that of CAF (Guo et al., 2017).

The observed pseudo first-order rate constants (k'_{obs}) of PRM and CAF degradation in the UV/chlorine process (determined from the first 5 min of reaction) were 0.187 and 0.339 min^{-1}, respectively. Our results are several times higher or comparable compared to those from previous studies (Guo et al., 2017; Wang et al., 2020), while the difference among the k'_{obs} values could be attributed to the use of

different experimental setup and conditions (Table S3). Comparison using an equal molar dose of FC or H_2O_2 under UV exposure showed that UV/chlorine exhibited a much higher removal efficacy for both contaminants. The k'_{obs} values for PRM and CAF were 3.96 and 7.72 times of those obtained from the UV/H_2O_2 process, respectively. Higher performance of UV/chlorine in CAF degradation in buffered ultrapure water, natural water, and wastewater effluent has been reported, owing to the formation of high $ClO^{\bullet}$ content (~3 orders of magnitude higher than that of $^{\bullet}OH$) in the UV/chlorine process and its preferential attack toward CAF (Yang et al., 2016; Guo et al., 2018; Wang et al., 2019). Our previous study also observed a better removal of PRM in the UV/chlorine process under similar experimental conditions at pH 7, where RCS species dominated ~55% of PRM decay kinetics (Wang et al., 2020). Conflicting result was obtained for PRM decay by Guo et al. (2018) using a mixture of 28 PPCPs at 1 μg L^{-1} with 2 mM PBS where UV/H_2O_2 demonstrated a better performance. This contradiction may be attributed to the different scavenging capacity of PBS exerted on the kinetics of contaminant degradation (i.e., single contaminant of mg L^{-1} level vs. mixture of μg L^{-1} level with a similar PBS).

In the UV/chlorine process, FC serves as the precursor and also major scavenger (including Cl^- from the FC stock) of $^{\bullet}OH$ and $Cl^{\bullet}$, meanwhile secondary $ClO^{\bullet}$ and $Cl_2^{\bullet-}$ radicals were produced through the scavenging effect (see reactions 38, 40, 41, 65, and 68 in Table S1). As FC increased from 10 to 35 μM, the modelled steady-state contents of $^{\bullet}OH$ and $Cl^{\bullet}$ increased from 3.3×10^{-14} M to 8.8×10^{-14} M and from 1.6×10^{-14} M to 2.4×10^{-14} M, and then maintained at ~1.3×10^{-13} M and 2.6×10^{-14} M in

the FC range of 70 - 210 μM (Figure S3), respectively. In contrast, continuous increase in $ClO^{\bullet}$ (10^{-10} - 10^{-9} M) and $Cl_2^{\bullet-}$ (10^{-15} - 10^{-14} M) concentration was observed at FC dose of 70 - 210 μM due to the conversion from $^{\bullet}OH$ and $Cl^{\bullet}$. Obviously, variation in FC dose remarkably changed the speciation of radical species, which in turn induced divergent degradation kinetics of PPCPs based on their reactivity toward specific radical species. As shown in Figure 2a, k'_{obs} of PRM exhibited a first increase and then reached a plateau similar to those of $^{\bullet}OH$ and $Cl^{\bullet}$ with increasing FC dose, while k'_{obs} of CAF linearly increased by 8.9-fold with the increase of FC from 10 to 210 μM, following a similar evolution profile of $ClO^{\bullet}$ and $Cl_2^{\bullet-}$.

Increase in initial contaminant concentration resulted in a decrease in k'_{obs} as shown in Figure 2b, likely attributed to the enhanced demand for reactive radicals at higher contaminant concentration. However, k'_{obs} of PRM just slightly decreased from 0.187 to 0.109 min^{-1} with the increase of initial concentration from 2 to 50 μM, while k'_{obs} of CAF exhibited an exponential decline from 1.022 to 0.041 min^{-1}. Kinetic modelling showed a decline in steady-state concentrations of both $^{\bullet}OH$ and RCS (Figure S4). However, $ClO^{\bullet}$ content was more significantly affected than other radical species and was reduced by ~3 orders of magnitude with increasing contaminant concentration from 2 to 50 μM. Consequently, the degradation of CAF dominated by $ClO^{\bullet}$ oxidation was remarkably inhibited at higher initial contaminant concentration. Besides, high concentration of CAF solution induced a much higher UV absorbance at 254 nm (0.205 at 1 cm for 50 μM CAF), while it was negligible for PRM (<0.01). The enhanced inner filter effect at high CAF concentration also contributed to its

292 sharp decline in decay rate constants.

293 **3.2 Elucidation of reactive species during UV/chlorine treatment**

294 Figure 3 depicts the specific k'_{obs} of UV light, chlorination, $^{\bullet}OH$, and RCS for
295 PRM and CAF degradation in the pH range of 6.2-9 based on the loss of NB i.e., in
296 *situ* $^{\bullet}OH$ probe (Figure S5, calculation detailed in SI Text S5). Contributions of direct
297 photolysis and chlorination to the decay of PRM/CAF were negligible. The
298 UV/chlorine treatment demonstrated a considerably higher decay kinetics in CAF
299 removal across pH 6.2-9 than that of PRM, which was rational considering the
300 comparable rate constants of CAF with $^{\bullet}OH$ but much higher reactivity toward the
301 main RCS species compared to PRM (rate constants of contaminants with $^{\bullet}OH$ and
302 RCS are provided in Table S4). Both PRM and CAF exhibited a decreasing trend in
303 k'_{obs} with increasing solution pH, consistent with previous literature (Sun et al., 2016;
304 Guo et al., 2017; Wang et al., 2020). Given that PRM (pK_a of 12.3) and CAF (pK_a of
305 6.1 and 10.4) occurred mainly as one speciation form under the investigated pH range,
306 the shift in chlorine speciation from HOCl toward ClO^- species with lower quantum
307 yield and higher scavenging effect on $^{\bullet}OH$ and $Cl^{\bullet}$ was the main reason accounting for
308 the decreased efficiency at elevated pH (Watts and Linden, 2007; Fang et al., 2014).
309 Meanwhile, pH variation exerted a negligible impact on the steady-state concentration
310 of $ClO^{\bullet}$ (Wu et al., 2017). For PRM, both $^{\bullet}OH$ and RCS were importantly involved in
311 the decay process at pH 6.2, and contribution of $^{\bullet}OH$ (i.e., 53%) was even slightly
312 higher than that of RCS (Figure S6). However, as the pH increased from 6.2 to 9, $k'_{^{\bullet}OH}$
313 for PRM significantly decreased by 80% whereas k'_{RCS} slightly increased from pH 6.2

to 7 and then kept constant at higher pH, indicating the predominant role of $ClO^{\bullet}$ and negligible role of $Cl^{\bullet}$ in alkaline conditions. For CAF, both $k'_{\bullet OH}$ and k'_{RCS} decreased with increasing pH. RCS dominated the degradation of CAF across pH 6.2-9, contributing to 72.9% of k'_{obs} at pH 6.2 and 86% - 87.8% at neutral to alkaline conditions (Figure S6). These results confirmed that the degradation of CAF was primarily attributable to RCS and particularly $ClO^{\bullet}$ oxidation.

3.3 Effects of anions

Figure 4 illustrates the impact of Cl^-, HCO_3^-, and NO_3^- on PRM and CAF degradation kinetics by the UV/chlorine treatment at pH 7. The presence of Cl^- induced a negligible inhibition on the k'_{obs} of both PPCPs, in agreement with Sun et al. (2016) and Wang et al. (2020). According to eqs. 1 and 2 (Grebel et al., 2010; Wu et al., 2016), formation of $Cl_2^{\bullet-}$ would be enhanced through the scavenging of $Cl^{\bullet}$ by Cl^-, while $^{\bullet}OH$ was not significantly affected with the addition of Cl^- due to the rapid reversible dissociation of $HOCl^{\bullet-}$ back into $^{\bullet}OH$. Kinetic modelling demonstrates the role of Cl^-, where 3 orders of magnitude increase in $Cl_2^{\bullet-}$ concentration, 36%-53% decrease in $Cl^{\bullet}$, and insignificant variation in $^{\bullet}OH$ and $ClO^{\bullet}$ were obtained in the presence of 10 mM Cl^- compared with the control. Given the above variations of main radical species in the system and the rate constants of two PPCPs with $^{\bullet}OH$ and RCS (see Table S4), the negligible inhibition on PRM/CAF degradation in the presence of Cl^- was probably due to that the increased contributions of $Cl_2^{\bullet-}$ compensated for the decrease of $Cl^{\bullet}$.

$$Cl^- + Cl^{\bullet} \leftrightarrow Cl_2^{\bullet-} \qquad k_{for} = 6.5 \times 10^9\ M^{-1}s^{-1},\ k_{res} = 1.1 \times 10^5\ s^{-1} \qquad (1)$$

$Cl^- + {}^{\bullet}OH \leftrightarrow HOCl^{\bullet-}$ $k_{for} = 4.3 \times 10^9\ M^{-1}s^{-1}$, $k_{res} = 6.1 \times 10^9\ M^{-1}s^{-1}$ (2)

The ubiquitous HCO_3^- presence in aquatic systems serves as important sink of $^{\bullet}OH$, $Cl^{\bullet}$, and $Cl_2^{\bullet-}$ through eqs. 3-5 (Fang et al., 2014), resulting in a decrease of these radical species as well as significant buildup of selective carbonate radical ($CO_3^{\bullet-}$). Modelling results showed that 10 mM HCO_3^- scavenged approximately 57% $^{\bullet}OH$, 89% $Cl^{\bullet}$, and 99% $Cl_2^{\bullet-}$, while $ClO^{\bullet}$ remained almost unchanged due to its low reactivity with HCO_3^- (Table S5). The steady-state concentration of $CO_3^{\bullet-}$ was simulated at level of 10^{-9} M, several orders of magnitude higher than those of $^{\bullet}OH$ and $Cl^{\bullet}$. The role of $CO_3^{\bullet-}$ in the degradation of micropollutants is compound-specific. Both PRM and CAF react with $CO_3^{\bullet-}$ at a low second-order rate constants ($<10^{-6}\ M^{-1}s^{-1}$, Text S6 and Figure S7) (Wu et al., 2017). Consequently, HCO_3^- induced an inhibitory effect on PRM and CAF degradation in the UV/chlorine process. As HCO_3^- increased from 0 to 10 mM HCO_3^-, k'_{obs} of PRM and CAF decreased from 0.186 to 0.113 min^{-1}, from 0.339 to 0.230 min^{-1}, respectively.

$HCO_3^- + {}^{\bullet}OH \rightarrow H_2O + CO_3^{\bullet-}$ $k = 8.5 \times 10^6\ M^{-1}s^{-1}$ (3)

$HCO_3^- + Cl^{\bullet} \rightarrow + H^+ + Cl^- + CO_3^{\bullet-}$ $k = 2.2 \times 10^8\ M^{-1}s^{-1}$ (4)

$HCO_3^- + Cl_2^{\bullet-} \rightarrow 2Cl^- + H^+ + CO_3^{\bullet-}$ $k = 8.0 \times 10^7\ M^{-1}s^{-1}$ (5)

In contrast to Cl^- and HCO_3^-, the presence of NO_3^- promoted the loss of PRM and CAF. This could be explained by the extra generation of $^{\bullet}OH$ and reactive nitrogen species (RNS, e.g., $NO_2^{\bullet}$) induced by photolysis of NO_3^- (Mack and Bolton, 1999). Experiments using NB as a $^{\bullet}OH$ probe confirmed the increasing contribution of $^{\bullet}OH$ to the decay kinetics of both PPCPs with the increase of NO_3^- (Figure S8) in the

353 UV/chlorine process. The $k'_{RCS+RNS}$ of CAF significantly increased with increasing
354 NO_3^-, while that of PRM kept almost constant. Degradation of PRM and CAF in the
355 UV/NO_3^- system (see Figure S8) showed that $^{\bullet}OH$ radical dominated the decay of
356 contaminants, followed by RNS. Meanwhile k'_{RNS} of CAF increased from 0.07 to 0.11
357 min^{-1} with the increase of NO_3^- from 50 to 100 mM, while k'_{RNS} of PRM kept constant.
358 Nevertheless, experimental results suggest a negligible enhancement from NO_3^- under
359 common WWTP effluent condition where concentration of NO_3^- is generally below 1
360 mM.

361 **3.4 Radical chemistry in simulated EfOM-containing water**

362 The degradation of PRM and CAF by UV/chlorine decreased with an increase in
363 EfOM concentration (Figure 5a-d). Both EfOM isolates inhibited the decay of CAF to
364 a substantial higher extent compared with that of PRM. Meanwhile, based on the
365 same DOC concentration, HPO fraction has a stronger impact on the degradation
366 kinetics of both contaminants than TPI fraction. The k'_{obs} of PRM reduced by 65.0%
367 and 31.7% in the presence of 10 mg-C L^{-1} HPO and TPI (Figure S9), respectively,
368 whereas that for CAF was 95.7% and 90.1%, respectively. These experimental results
369 indicate that the radical chemistry in the UV/chlorine system varied in the presence of
370 different EfOM isolates. The two EfOM isolates bearing different physicochemical
371 properties likely account for their different influence. The SUVA values of HPO and
372 TPI were determined as 3.10 and 1.96 L mg^{-1} m^{-1}, respectively. HPO with higher
373 SUVA is more enriched in aromatic moieties than TPI considered as more hydrophilic
374 in nature with a higher abundance of aliphatic carbon (Weishaar et al., 2003). The

good correlations (linear for PRM and exponential for CAF) obtained between UV absorbance at 254 nm and k'_{obs} for all HPO and TPI solutions (Figure 6) demonstrate that the larger the presence of aromatic moieties into the solution the stronger the inhibition of the degradation of targeted contaminants by the UV/chlorine process. Figure 6 confirms that the presence of UV absorbing moieties has a stronger effect on CAF degradation compared to PRM.

Figure 5e compares the impact of the two EfOM isolates at 5 mg-C L^{-1} on the contribution of $k'_{\bullet OH}$ and k'_{RCS} for PRM and CAF decay at pH 7. It can be seen that decay of contaminants due to RCS oxidation was significantly inhibited in comparison with the moderate decrease in $k'_{\bullet OH}$, suggesting that RCS is more vulnerable to EfOM. Typically, k'_{RCS} for CAF dropped by ~94.5%, contributing to approximately 82.5% of the total loss in k'_{obs}. Since the decay of CAF is primarily due to $ClO^{\bullet}$, EfOM isolates preferentially scavenging $ClO^{\bullet}$ could be the main reason causing the sharp decline of k'_{RCS} for CAF. The scavenging capacity of DOM isolates on $ClO^{\bullet}$ shows a strong dependency upon SUVA (Wang et al., 2020). As a result, at pH 7 where $ClO^{\bullet}$ dominated the decay of PPCPs, HPO fraction induced a higher degree of inhibition on the UV/chlorine process. The reactivity of DOM (EfOM) with $Cl_2^{\bullet-}$ was also found to be positively correlated with aromatic carbon content (i.e., SUVA) (Lei et al., 2021). The role of physicochemical properties of EfOM in the reactivity toward $^{\bullet}OH$ and $Cl^{\bullet}$ is complicated, as some nonaromatic moieties (e.g., thiols and sulfonate group) of EfOM in addition to aromatic components exhibit high vulnerability to $^{\bullet}OH$ or $Cl^{\bullet}$ attack (Westerhoff et al., 2007; Varanasi et al., 2018). No

correlation was found between SUVA and rate constants of DOM with $Cl^{\bullet}$ (Lei et al., 2021). Studies on the relationship of SUVA with $^{\bullet}OH$ rate constants of EfOM (i.e, $k_{\bullet OH, EfOM}$) remain inconsistent. Keen et al. (2014) observed some correlation (R^2 = 0.75) between SUVA and $k_{\bullet OH, EfOM}$, while Westerhoff et al. (2007) found no strong statistical relevant trend.

The presence of 5 mg-C L^{-1} EfOM resulted in significantly faster consumption of FC in the UV/chlorine process. As shown in Figure 5f, the chlorine residual was barely detected in 10 min for HPO and TPI in the UV/chlorine process. In comparison, photolysis of FC without EfOM only consumed 21% of FC, while dark chlorination of the two EfOM isolates led to less than 46% decay of FC. HPO with higher SUVA exhibits a higher chlorine demand, in agreement with previous studies (Westerhoff et al., 2004; Wang et al., 2020). Besides, SUVA of EfOM causes light absorption during the UV/chlorine process. The higher the SUVA, the stronger the light attenuation. The applied UV fluence was reduced by 21.3% and 14.2% in the presence of 5.0 mg-C L^{-1} HPO and TPI, respectively. The above effects from EfOM play additional roles in lowering the steady-state concentration of radicals, therefore reducing the process efficiency and driving the different impact of EfOM with diverse properties.

3.5 Degradation in real and reconstituted WWTP effluent

The degradation of PRM and CAF in real WWTP effluent and in reconstituted effluent by adding the major matrix components (i.e., HPO and TPI EfOM isolates added in representative relative abundance, Cl^-, HCO_3^-, and NO_3^-) based on the real wastewater effluent quality (see Table S6) was investigated. Preliminary experiments

419 demonstrated an insignificant role of UV-induced photolysis of PRM and CAF in
420 WWTP effluent (Figure S10). As illustrated in Figure 7a and 7b, the degradation of
421 PRM and CAF was retarded when UV/chlorine was applied to WWTP effluent,
422 showing a strong scavenging effect from the wastewater matrix. Compared to the
423 control, k'_{obs} of PRM was reduced by 43.3%. Specifically, the decay kinetics of CAF
424 was almost completely suppressed (>90%) in WWTP effluent. Additionally, the
425 relatively high EfOM content (6.07 mg-C L^{-1}) in WWTP effluent led to a rapid
426 depletion (>95%) of 70 μM FC in 4 min (Figure S11) through the synergistic effects
427 of directly reacting with FC and accelerating its photolysis. As a result, a rapid decay
428 of PRM in the first 4 min followed by a retardation decay stage was observed.
429 Increasing FC dose can progressively offset the inhibitory effect by providing more
430 chlorine residual (Figure S11 and S12). The removals obtained at chlorine dose of 210
431 μM for PRM and CAF were 79.4% and 75.0%, respectively, while they were 40.4%
432 and 14.2% at 70 μM FC. Contributions of $k'_{\bullet OH}$ and k'_{RCS} to PRM/CAF decay both
433 increased with the increase of FC dose (Figure 7c).

434 Results obtained with reconstituted effluent are comparable to the ones obtained
435 with real WWTP effluent, suggesting that the major influencing factors inhibiting the
436 PPCPs removal were taken into account. It is important to note that the reconstituted
437 effluent was prepared by adding similar quantities of HPO and TPI (same amount of
438 HPO and TPI were isolated from WWTP effluent) to obtain the same UV_{254}
439 absorbance as the real WWTP effluent (i.e., 0.133; 1 cm). The strong inhibitory effect
440 of the water matrix could be mainly attributed to the relatively high EfOM content

441 (DOC # 6 mg L^{-1}) and alkalinity (3.6 mM), as organics and HCO_3^- both adversely
442 lower the process efficiency. The results obtained with the two waters fit well to the
443 correlation between k'_{obs} and UV absorbance at 254 nm established in Figure 6. This
444 observation provides evidence that the presence of organic matter and more
445 specifically UV absorbing organic moieties, is likely the predominant factor affecting
446 the UV/chlorine process in this WWTP effluent. These findings demonstrate that
447 EfOM isolates can be used to determine the efficiency of the UV/chlorine process in
448 real effluent. Nevertheless, we speculate that using HPO and TPI EfOM isolates
449 (which represent around 50% of the DOC and more than 80% of UV absorbance) to
450 simulate the whole DOC in real effluent may slightly magnify the reactive EfOM
451 fraction, as the XAD® resin protocol cannot effectively extract the hydrophilic or very
452 polar nonaromatic organics which generally have less reactivity toward free chlorine
453 and radicals.

454 Compared with WWTP effluent, decay of PRM and CAF was obviously
455 enhanced in tap water, leading to 66.0% and 75.6% of removal, respectively. It can be
456 concluded that in waters with low levels of impurities after removing DOC and
457 alkalinity or even in complex wastewater effluent with sufficient chlorine residual
458 supply, UV/chlorine is a promising alternative for PPCPs elimination.

459 **3.6 Toxicity assessment**

460 Previous studies have drawn inconsistent findings on the associations between
461 AOX concentration and toxicity. Chlorinated byproducts were reported to correlate
462 with the variation in the toxicity during UV/chlorine and chlorination treatment of

463 trimethoprim (Wu et al., 2016). The evolution of chlorine-containing intermediates
464 showed no relationship with toxicity changes in the degradation of gemfibrozil by
465 UV/chlorine (Kong et al., 2018). Wang et al. (2017) found that cytotoxicity positively
466 correlated with AOX formation based on the comparison between UV/chlorine and
467 chlorination treatment of natural organic matter, but weakly related to AOX
468 concentrations by comparing among different reaction times. In our study, attempt
469 was also made to evaluate the AOCl formation in the context of potential toxicity.
470 Figure 8 presents the formation of AOCl after 10 min of UV/chlorine treatment.
471 Significant formation of AOCl was observed in the presence of 5 mg-C L^{-1} EfOM
472 isolate, i.e., 7.51 and 5.94 μM from HPO and TPI, respectively. The addition of 5 μM
473 contaminant induced negligible impact on the yield of AOCl. High resolution LC/MS
474 and GC/MS analyses of the SPE extracts did not provide any evidence of the presence
475 of chlorinated by-products for both PRM and CAF under the applied experimental
476 conditions. Lists of identified transformation intermediates are provided in Table S7
477 and S8. It should be noted that the applied analytical methods were not appropriate to
478 analyze low molecular weight chlorinated by-products that could account for the
479 produced AOCl.

480 Considering the production of intermediates and chlorinated by-products in the
481 presence of EfOM isolate, evaluation of the risk caused by the UV/chlorine process is
482 of great significance. Therefore, different toxic effects of treated samples on HepG2
483 cells were investigated.

484 As shown in Figure 9a, compared to experimental controls (PBS), a significant

485 increase in the cellular oxidative stress was observed for most experiments containing
486 HPO. The untreated HPO showed a (4.1±0.4)-fold increase in ROS signal over the
487 negative control ($P<0.0001$), which was much higher than the TPI fraction. Higher
488 toxicity of HPO EfOM than TPI was also reported (Le Roux et al., 2017). Both
489 UV/Cl_2+HPO+PRM (1.9±0.2, $P<0.005$) and UV/Cl_2+HPO+CAF (2.97 ± 0.6,
490 $P<0.0001$) extracts showed a significantly increased ROS production; fold change for
491 UV/Cl_2+HPO was not statistically significant. The induction of oxidative stress
492 response pathway is an indicator of the presence of chemical and non-chemical
493 stresses in cells, and, for water samples, it is believed that most oxidative stress
494 response comes from unknown chemicals (Escher et al., 2013). Many DPBs have
495 been implicated with the increase in adaptive stress responses following water
496 disinfection, toxicity is also highly dependent on treatment technique and disinfection
497 mechanism (Lundqvist et al., 2019). In our study, UV/chlorine treatment of the
498 contaminants did not significantly alter the oxidative stress. On the other hand, the
499 presence of PRM and CAF seems to hinder the reduction of HPO cellular ROS
500 production. We believe that these compounds are consuming a significant part of the
501 radicals produced which will not react with the PPCPs or other unknown chemicals
502 initially present in the HPO or TPI isolate. The targeted 11 PPCPs (not necessarily
503 considered as responsible for the toxicity of EfOM isolates) were present in the
504 untreated EfOM isolates and the UV/chlorine treatment of EfOM isolate generally
505 degrade these PPCPs to a certain extent (Table S9).
506 As an early and sensitive indicator, ROS plays critical roles in cell survival,

apoptosis, and death (Franklin, 2011). Previous studies showed that the gene expression pathways of monohaloacetic acids-treated cells would be modulated through the generation of ROS, causing DNA damage, ATP depletion and mitochondrial stress (Dad et al., 2013). Oxidative stress is one of the main causes of genotoxic insults together with exposure to UV irradiation and chemicals. Induction of pH2AX, a sensitive molecular marker of DNA damage and repair (Mei et al., 2015), is associated with double-strand breaks (DSBs) and is among the most serious forms of DNA damage that can lead to cellular death, chromosomal aberrations, mutations, and cancer (Mah et al., 2010). While exposure to HPO and TPI had no significant effect on cell DNA damage, as measured by pH2AX induction, treatments with UV/Cl_2+HPO (fold change 2.2±0.5, P=0.0003), UV/Cl_2+HPO+PRM (fold change 3.0±0.7, P<0.0001), UV/Cl_2+HPO+CAF (fold change 4.1±0.8, P<0.0001), and UV/Cl_2+TPI+CAF (fold change 1.9 ± 0.4, P=0.0081) all showed a significant fold change for pH2AX induction (Figure 9b). Similar effects were also observed for chlorination only samples, with an increased role of HPO over TPI; a pH2AX induction of Cl_2+HPO sample fold change of 2.2±0.3 versus Cl_2+TPI sample fold change of 1.7±0.5, and a ROS induction of 2.1±0.3 versus 0.9±0.2, respectively (data not shown in graph).

While oxidative stress results for UV treated samples showed similar patterns, as those for pH2AX induction assay, the lack of DNA damage for HPO-only sample suggests that cellular ROS and oxidative stress are not the only factors responsible for the increase in pH2AX induction. The induction of genotoxic effects by different

mechanisms was demonstrated by different studies on drinking water treatment processes (Lundqvist et al., 2019), and strands breaks have been shown to be caused by halogenated DBPs such as trihalomethanes (Geter et al., 2004).

To confirm the induction of oxidative stress caused by the tested samples, mitochondrial function assays were employed. ROS levels and mitochondrial function are closely related. Exogenous stimuli can induce mitochondrial ROS production, and oxidative stress causes the collapse of mitochondrial membrane potential, resulting in an increase in ROS in a positive feedback loop (ROS-induced ROS release) (Zorov et al., 2000). HPO-only, UV/Cl_2+HPO+PRM and UV/Cl_2+HPO+CAF extracts have a generalized effect of mitochondrial dysfunction, affecting different stages of the electron transport chain and reducing basal respiration, maximal respiration, and ATP production levels (Figure 9c and Figures S13). This effect is consistent with previously observed effects from induced oxidative stress (Zorov et al., 2006), and different studies showed similarly related mitochondrial-dependent toxicity through oxidative stress for different DBPs (Zuo et al., 2017).

As a sum parameter of overall toxicity, cytotoxicity serves as the overarching effect overlying each of the cellular toxicity pathways (Escher et al., 2014). No significant cytotoxicity was observed at the concentration (20x) used for oxidative stress, mitochondrial function, and DNA damage assays. General cell cytotoxicity was observed at higher exposure concentration (40x) for UV/Cl_2+HPO+PRM and UV/Cl_2+HPO+CAF samples possibly due to the increased DNA damage, mitochondrial and oxidative stress.

Taken together, the observations demonstrate that chlorinated byproducts could induce oxidative stress, mitochondrial dysfunction, and increase DNA damage. The nature of EfOM present seems to be the predominant factor affecting toxicity and the presence of different model compounds such as PRM and CAF shows that the UV/chlorine treatment can have preferential targets that also impact in the overall toxic effects. Although AOCl results are consistent for all isolate samples, the composition of AOCl fraction can have a great impact on cellular toxicity (Du et al., 2020). The mechanism of action observed in our study, involving cytotoxicity, oxidative stress, mitochondrial dysfunction, and DNA damage are also comparable to previous studies (Wang et al., 2018).

4. Conclusion

The UV/chlorine process was efficient for degrading UV- and chlorine-resistant PPCPs due to the generation of radical species. The decay of PRM and CAF was maximized at pH 6.2 and decreased with increasing solution pH. Both $^{\bullet}OH$ and RCS dominated the decay of PRM at acidic pH, while contribution of RCS became more important at alkaline condition. The loss of CAF was mainly attributed to $ClO^{\bullet}$. The variation of chlorine dose and initial concentration of contaminant significantly alters the content of $ClO^{\bullet}$, thereby leading to a more pronounced influence on the decay of CAF. The k'_{obs} for PRM and CAF degradation was not apparently impacted by Cl^- ions but suppressed with the increase of HCO_3^- concentration, while NO_3^- enhanced the process efficiency through the extra generation of $^{\bullet}OH$ and RNS.

Degradation of PRM and CAF by UV/chlorine decreased with an increase in

EfOM concentration. The HPO fraction with higher SUVA has a stronger impact than the TPI fraction. The presence of EfOM has a stronger inhibition on CAF degradation compared to that of PRM by preferentially scavenging $ClO^{\bullet}$. Good correlations (linear for PRM and exponential for CAF) were obtained between k'_{obs} of contaminants and UV absorbance at 254 nm of all EfOM solutions including the real effluent and reconstituted effluent, suggesting that the UV absorbing organic moieties in EfOM is likely the predominant factor affecting the UV/chlorine process in WWTP effluent.

The presence of EfOM isolate serves as important precursors of AOCl during UV/chlorine treatment, which induced significant effect on cellular DNA damage. A remarkable increase in intracellular oxidative stress was observed for most experiments containing HPO, while UV/chlorine treatment did not induce a significant increase in oxidative stress in our study, suggesting the nature of EfOM has a significant impact on the cytotoxicity.

Acknowledgments

This research was supported by the Fundamental Research Funds for the Central Universities (GK202103145), Natural Science Basic Research Plan of Shaanxi Province (2021JM-192), Experimental Technology Research Project of SNNU (SYJS202114), and Special Financial Grant from Shaanxi Postdoctoral Science Foundation (No.2017BSHTDZZ09).

References:

Beitz, T., Beckmann, W. and Mitzner, R. (1998) Investigations of reactions of selected azaarenes with radicals in water. 2. chlorine and bromine radicals. J. Phys. Chem. A 102(34), 6766-6771.

Bolton, J.R., Stefan, M.I., Shaw, P.-S. and Lykke, K.R. (2011) Determination of the quantum

yields of the potassium ferrioxalate and potassium iodide-iodate actinometers and a method for the calibration of radiometer detectors. J. Photochem. Photobiol. A: Chem. 222(1), 166-169.

Bulman, D.M. and Remucal, C.K. (2020) Role of Reactive Halogen Species in Disinfection Byproduct Formation during Chlorine Photolysis. Environ. Sci. Technol. 54(15), 9629-9639.

Buxton, G.V., Greenstock, C.L., Helman, W.P. and Ross, A.B. (1988) Critical review of rate constants for reactions of hydrated electrons, hydrogen atoms and hydroxyl radicals ($^{\bullet}OH/^{\bullet}O^{-}$) in aqueous solution. J. Phys. Chem. Ref. Data 17(2), 513-886.

Cheng, S., Zhang, X., Yang, X., Shang, C., Song, W., Fang, J. and Pan, Y. (2018) The Multiple Role of Bromide Ion in PPCPs Degradation under UV/Chlorine Treatment. Environ. Sci. Technol. 52(4), 1806-1816.

Crittenden, J.C., Trussell, R.R., Hand, D.W., Howe, K.J. and Tchobanoglous, G. (2005) Water treatment: Principles and Design, John Wiley & Sons, Inc., New Jersey, USA.

Croué, J.-P. and Reckhow, D.A. (1989) Destruction of chlorination by-products with sulphite. Environ. Sci. Technol. 23, 1412-1419.

Dabrowski, L. (2016) Review of use of keepers in solvent evaporation procedure during the environmental sample analysis of some organic pollutants. Trac-Trends in Analytical Chemistry 80, 507-516.

Dad, A., Jeong, C.H., Pals, J.A., Wagner, E.D. and Plewa, M.J. (2013) Pyruvate remediation of cell stress and genotoxicity induced by haloacetic acid drinking water disinfection by-products. Environ Mol Mutagen 54(8), 629-637.

Drewes, J.E. and Croué, J.P. (2002) New approaches for structural characterization of organic matter in drinking water and wastewater effluents. Water Supply 2(2), 1-10.

Du, Y., Wang, W.-L., He, T., Sun, Y.-X., Lv, X.-T., Wu, Q.-Y. and Hu, H.-Y. (2020) Chlorinated effluent organic matter causes higher toxicity than chlorinated natural organic matter by inducing more intracellular reactive oxygen species. Science of The Total Environment 701, 134881.

Escher, B.I., Allinson, M., Altenburger, R., Bain, P.A., Balaguer, P., Busch, W., Crago, J., Denslow, N.D., Dopp, E., Hilscherova, K., Humpage, A.R., Kumar, A., Grimaldi, M., Jayasinghe, B.S., Jarosova, B., Jia, A., Makarov, S., Maruya, K.A., Medvedev, A., Mehinto, A.C., Mendez, J.E., Poulsen, A., Prochazka, E., Richard, J., Schifferli, A., Schlenk, D., Scholz, S., Shiraishi, F., Snyder, S., Su, G., Tang, J.Y., van der Burg, B., van der Linden, S.C., Werner, I., Westerheide, S.D., Wong, C.K., Yang, M., Yeung, B.H., Zhang, X. and Leusch, F.D. (2014) Benchmarking organic micropollutants in wastewater, recycled water and drinking water with in vitro bioassays. Environ Sci Technol 48(3), 1940-1956.

Escher, B.I., van Daele, C., Dutt, M., Tang, J.Y.M. and Altenburger, R. (2013) Most Oxidative Stress Response In Water Samples Comes From Unknown Chemicals: The Need For Effect-Based Water Quality Trigger Values. Environmental Science & Technology 47(13), 7002-7011.

Fang, J., Fu, Y. and Shang, C. (2014) The Roles of Reactive Species in Micropollutant Degradation in the UV/Free Chlorine System. Environ. Sci. Technol. 48(3), 1859-1868.

Feng, Y., Smith, D.W. and Bolton, J.R. (2007) Photolysis of aqueous free chlorine species (HOCl and OCl^{-}) with 254 nm ultraviolet light. Journal of Environmental Engineering and

Science 6(3), 277-284.
Franklin, J.L. (2011) Redox Regulation of the Intrinsic Pathway in Neuronal Apoptosis. ANTIOXIDANTS & REDOX SIGNALING 14(8).
Geter, D.R., Chang, L.W., Hanley, N.M., Ross, M.K., Pegram, R.A. and DeAngelo, A.B. (2004) Analysis of in vivo and in vitro DNA strand breaks from trihalomethane exposure. J Carcinog 3(1), 2.
Grebel, J.E., Pignatello, J.J. and Mitch, W.A. (2010) Effect of Halide Ions and Carbonates on Organic Contaminant Degradation by Hydroxyl Radical-Based Advanced Oxidation Processes in Saline Waters. Environ. Sci. Technol. 44(17), 6822-6828.
Guo, K., Wu, Z., Shang, C., Yao, B., Hou, S., Yang, X., Song, W. and Fang, J. (2017) Radical Chemistry and Structural Relationships of PPCP Degradation by UV/Chlorine Treatment in Simulated Drinking Water. Environ. Sci. Technol. 51(18), 10431-10439.
Guo, K., Wu, Z., Yan, S., Yao, B., Song, W., Hua, Z., Zhang, X., Kong, X., Li, X. and Fang, J. (2018) Comparison of the UV/chlorine and UV/H_2O_2 processes in the degradation of PPCPs in simulated drinking water and wastewater: Kinetics, radical mechanism and energy requirements. Water Res. 147, 184-194.
Hamid, N., Junaid, M., Wang, Y., Pu, S.-Y., Jia, P.-P. and Pei, D.-S. (2021) Chronic exposure to PPCPs mixture at environmentally relevant concentrations (ERCs) altered carbohydrate and lipid metabolism through gut and liver toxicity in zebrafish. Environmental pollution (Barking, Essex : 1987) 273, 116494-116494.
Ianni, J.C. (2018) Kinetics. Windows Virsion 6.70., http://www.kintecus.com.
Ina, K., Arron, L., Cynthia, J. and Anna, H. (2014) To add or not to add: The use of quenching agents for the analysis of disinfection by-products in water samples. Water Res. 59, 90-98.
Keen, O.S., McKay, G., Mezyk, S.P., Linden, K.G. and Rosario-Ortiz, F.L. (2014) Identifying the factors that influence the reactivity of effluent organic matter with hydroxyl radicals. Water Res. 50, 408-419.
Kong, X., Wu, Z., Ren, Z., Guo, K., Hou, S., Hua, Z., Li, X. and Fang, J. (2018) Degradation of lipid regulators by the UV/chlorine process: Radical mechanisms, chlorine oxide radical (ClO center dot)-mediated transformation pathways and toxicity changes. Water Res. 137, 242-250.
Krasner, S.W., Westerhoff, P., Chen, B., Rittmann, B.E., Nam, S.-N. and Amy, G. (2009) Impact of Wastewater Treatment Processes on Organic Carbon, Organic Nitrogen, and DBP Precursors in Effluent Organic Matter. Environ. Sci. Technol. 43(8), 2911-2918.
Le Roux, J., Plewa, M.J., Wagner, E.D., Nihemaiti, M., Dad, A. and Croue, J.-P. (2017) Chloramination of wastewater effluent: Toxicity and formation of disinfection byproducts. Journal of Environmental Sciences 58, 135-145.
Lei, Y., Cheng, S., Luo, N., Yang, X. and An, T. (2019) Rate Constants and Mechanisms of the Reactions of Cl-center dot and Cl-2(center dot-) with Trace Organic Contaminants. Environ. Sci. Technol. 53(19), 11170-11182.
Lei, Y., Lei, X., Westerhoff, P., Zhang, X. and Yang, X. (2021) Reactivity of chlorine radicals ($Cl^{\bullet}$ and $Cl_2^{\bullet-}$) with dissolved organic matter and the formation of chlorinated byproducts. Environ. Sci. Technol. 55, 689-699.
Lundqvist, J., Andersson, A., Johannisson, A., Lavonen, E., Mandava, G., Kylin, H., Bastviken, D. and Oskarsson, A. (2019) Innovative drinking water treatment techniques reduce the

disinfection-induced oxidative stress and genotoxic activity. Water Research 155, 182-192.
Mack, J. and Bolton, J.R. (1999) Photochemistry of nitrite and nitrate in aqueous solution: a review. J. Photochem. Photobiol. A: Chem. 128(1999), 1-13.
Mah, L.J., El-Osta, A. and Karagiannis, T.C. (2010) γH2AX: a sensitive molecular marker of DNA damage and repair. Leukemia 24(4), 679-686.
Mei, L., Hu, Q., Peng, J., Ruan, J., Zou, J., Huang, Q., Liu, S. and Wang, H. (2015) Phospho-histone H2AX is a diagnostic and prognostic marker for epithelial ovarian cancer. Int J Clin Exp Pathol 8(5), 5597-5602.
Miklos, D.B., Wang, W.L., Linden, K.G., Drewes, E. and Huebner, U. (2019) Comparison of UV-AOPs (UV/H_2O_2, UV/PDS and UV/Chlorine) for TOrC removal from municipal wastewater effluent and optical surrogate model evaluation. Chem. Eng. J. 362, 537-547.
Moore, H.E., Garmendia, M.J. and Cooper, W.J. (1984) Kinetics of monochloramine oxidation of N,N-diethyl-p-phenylenediamine. Environ. Sci. Technol. 18(5), 348-353.
O'Connor, M., Helal, S.R., Latch, D.E. and Arnold, W.A. (2019) Quantifying photo-production of triplet excited states and singlet oxygen from effluent organic matter. Water Res. 156, 23-33.
Sun, P., Lee, W.-N., Zhang, R. and Huang, C.-H. (2016) Degradation of DEET and Caffeine under UV/Chlorine and Simulated Sunlight/Chlorine Conditions. Environ. Sci. Technol. 50(24), 13265-13273.
Varanasi, L., Coscarelli, E., Khaksari, M., Mazzoleni, L.R. and Minakata, D. (2018) Transformations of dissolved organic matter induced by UV photolysis, Hydroxyl radicals, chlorine radicals, and sulfate radicals in aqueous-phase UV-Based advanced oxidation processes. Water Res. 135, 22-30.
Wang, C., Moore, N., Bircher, K., Andrews, S. and Hofmann, R. (2019) Full-scale comparison of UV/H_2O_2 and UV/Cl_2 advanced oxidation: The degradation of micropollutant surrogates and the formation of disinfection byproducts. Water Res. 161, 448-458.
Wang, G., Wang, J., Zhu, L., Wang, J., Li, H., Zhang, Y., Liu, W. and Gao, J. (2018) Oxidative Damage and Genetic Toxicity Induced by DBP in Earthworms (Eisenia fetida). Arch Environ Contam Toxicol 74(4), 527-538.
Wang, W.-L., Zhang, X., Wu, Q.-Y., Du, Y. and Hu, H.-Y. (2017) Degradation of natural organic matter by UV/chlorine oxidation: Molecular decomposition, formation of oxidation byproducts and cytotoxicity. Water Res. 124, 251-258.
Wang, Y., Couet, M., Gutierrez, L., Allard, S. and Croue, J.-P. (2020) Impact of DOM source and character on the degradation of primidone by UV/chlorine: Reaction kinetics and disinfection by-product formation. Water Res. 172.
Watts, M.J. and Linden, K.G. (2007) Chlorine photolysis and subsequent OH radical production during UV treatment of chlorinated water. Water Res. 41(13), 2871-2878.
Weishaar, J.L., Aiken, G.R., Bergamaschi, B.A., Fram, M.S., Fujii, R. and Mopper, K. (2003) Evaluation of specific ultraviolet absorbance as an indicator of the chemical composition and reactivity of dissolved organic carbon. Environ. Sci. Technol. 37(20), 4702-4708.
Westerhoff, P., Chao, P. and Mash, H. (2004) Reactivity of natural organic matter with aqueous chlorine and bromine. Water Res. 38(6), 1502-1513.
Westerhoff, P., Mezyk, S.P., Cooper, W.J. and Minakata, D. (2007) Electron pulser radiolysis determination of hydroxyl radical rate constants with suwannee river fulvic acid and other

729 dissolved organic matter isolates. Environ. Sci. Technol. 41(13), 4640-4646.
730 Wu, Z., Fang, J., Xiang, Y., Shang, C., Li, X., Meng, F. and Yang, X. (2016) Roles of reactive
731 chlorine species in trimethoprim degradation in the UV/chlorine process: Kinetics and
732 transformation pathways. Water Res. 104, 272-282.
733 Wu, Z., Guo, K., Fang, J., Yang, X., Xiao, H., Hou, S., Kong, X., Shang, C., Yang, X., Meng, F.
734 and Chen, L. (2017) Factors affecting the roles of reactive species in the degradation of
735 micropollutants by the UV/chlorine process. Water Res. 126, 351-360.
736 Yang, X., Sun, J., Fu, W., Shang, C., Li, Y., Chen, Y., Gan, W. and Fang, J. (2016) PPCP
737 degradation by UV/chlorine treatment and its impact on DBP formation potential in real
738 waters. Water Res. 98, 309-318.
739 Yang, Y., Ok, Y.S., Kim, K.-H., Kwon, E.E. and Tsang, Y.F. (2017) Occurrences and removal of
740 pharmaceuticals and personal care products (PPCPs) in drinking water and water/sewage
741 treatment plants: A review. Sci. Total Environ. 596, 303-320.
742 Zorov, D.B., Filburn, C.R., Klotz, L.O., Zweier, J.L. and Sollott, S.J. (2000) Reactive oxygen
743 species (ROS)-induced ROS release: a new phenomenon accompanying induction of the
744 mitochondrial permeability transition in cardiac myocytes. J Exp Med 192(7), 1001-1014.
745 Zorov, D.B., Juhaszova, M. and Sollott, S.J. (2006) Mitochondrial ROS-induced ROS release:
746 an update and review. Biochim Biophys Acta 1757(5-6), 509-517.
747 Zuo, Y.-T., Hu, Y., Lu, W.-W., Cao, J.-J., Wang, F., Han, X., Lu, W.-Q. and Liu, A.-L. (2017)
748 Toxicity of 2,6-dichloro-1,4-benzoquinone and five regulated drinking water disinfection
749 by-products for the Caenorhabditis elegans nematode. Journal of Hazardous Materials 321,
750 456-463.
751
752

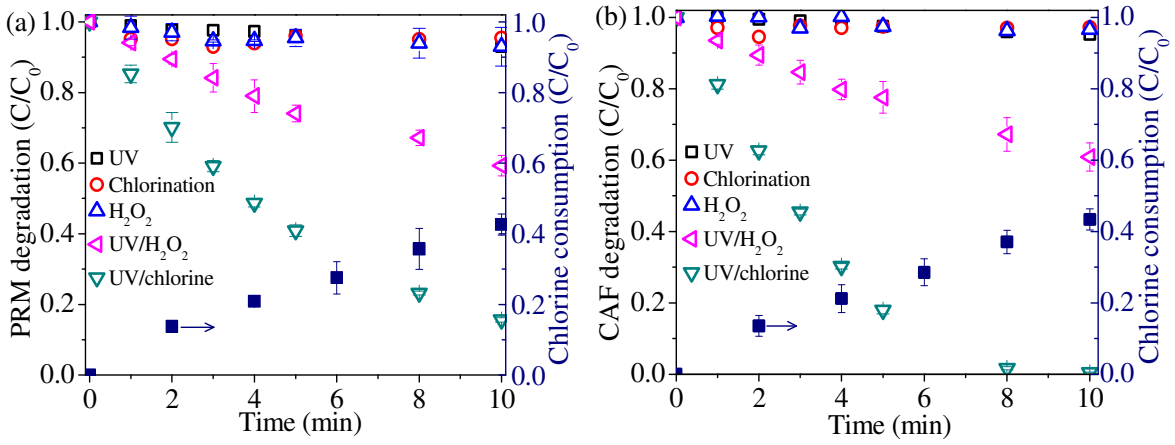

Figure 1. (a) PRM and (b) CAF degradation by UV irradiation, chlorination, H_2O_2 oxidation, UV/H_2O_2, and UV/chlorine processes; and the corresponding chlorine consumption in the UV/chlorine process. Conditions: [PRM] = [CAF] = 5 μM, [chlorine] = [H_2O_2] = 70 μM, pH = 7.

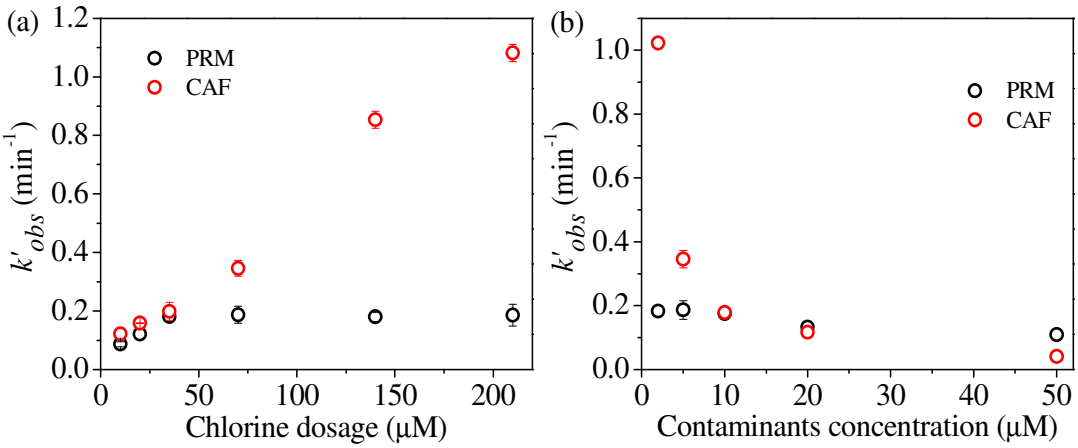

Figure 2. Observed rate constants (k'_{obs}) for PRM and CAF decay in the UV/chlorine process under (a) various chlorine dose and (b) PPCPs concentration. Conditions: (a) [PRM] = [CAF] = 5 μM, pH = 7; (b) [chlorine] = 70 μM, pH = 7.

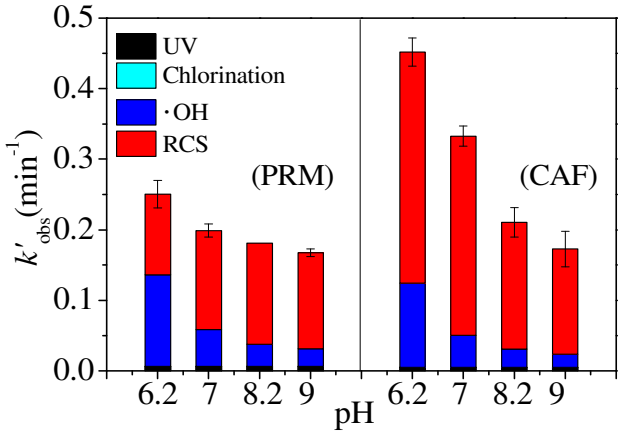

Figure 3. Observed rate constants (k'_{obs}) and contributions of specific species for PRM and CAF decay in the UV/chlorine process at different pH. Conditions: [PRM] = [CAF] = 5 μM, [chlorine] = 70 μM, [NB] = 1 μM.

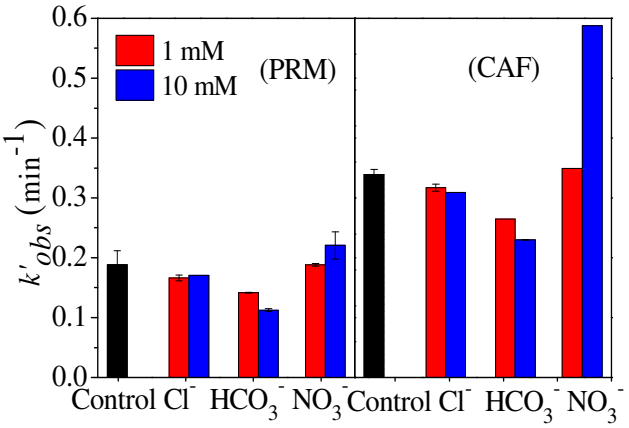

Figure 4. Effect of Cl^-, HCO_3^-, and NO_3^- on the degradation of PRM and CAF in the UV/chlorine process. Conditions: [PRM] = [CAF] = 5 μM, [chlorine] = 70 μM, pH = 7.

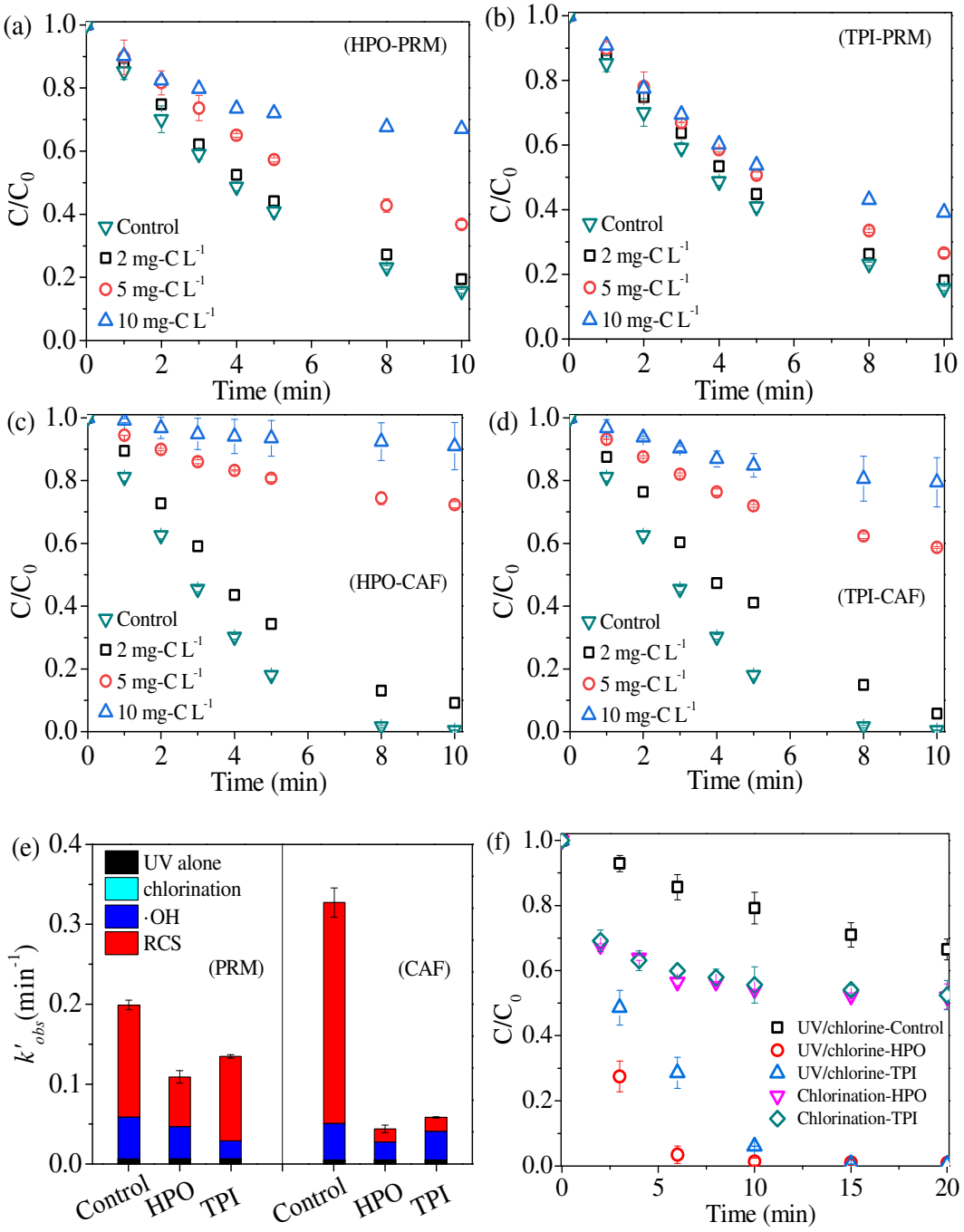

Figure 5. Effect of different concentrations of (a, c) HPO and (b, d) TPI on the degradation of PRM and CAF in the UV/chlorine systems; (e) effect of 5 mg-C L^{-1} EfOM isolate on the contribution of $k'_{\bullet OH}$ and k'_{RCS} for PRM and CAF decay at pH 7 with 1 μM NB as radical probe, and (f)

corresponding chlorine consumption during the UV/chlorine process in comparison with dark chlorination of EfOM isolates. Conditions: [PRM] = [CAF] = 5 μM, [chlorine] = 70 μM, pH = 7.

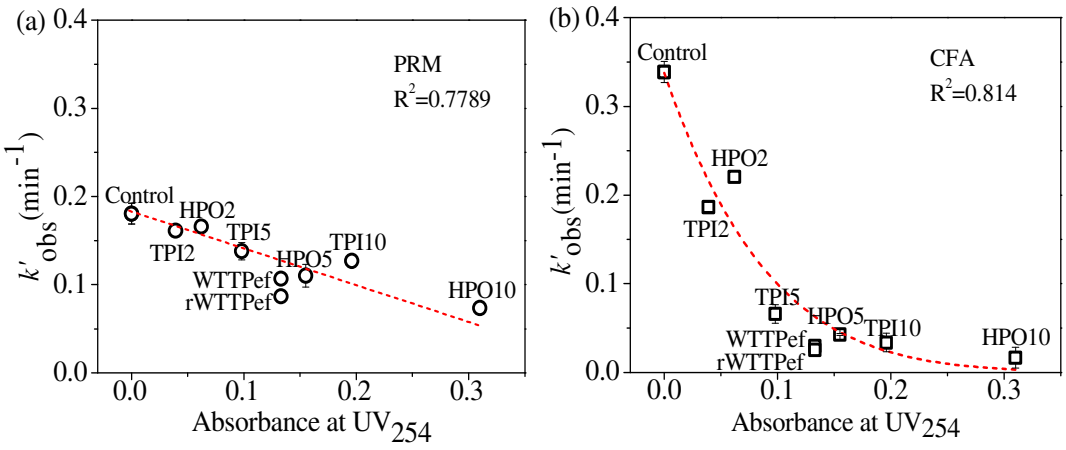

Figure 6. The linear correlation for (a) PRM and exponential correlation for (b) CAF obtained between the UV absorbance at 254 nm and k'_{obs} with all HPO and TPI solutions. HPO2-HPO10 and TPI2-TPI10 represent the solution with 2-10 mg-C L^{-1} of EfOM isolate, WTTPef and rWTTPef represent the WWTP effluent and reconstituted WTTP effluent, respectively.

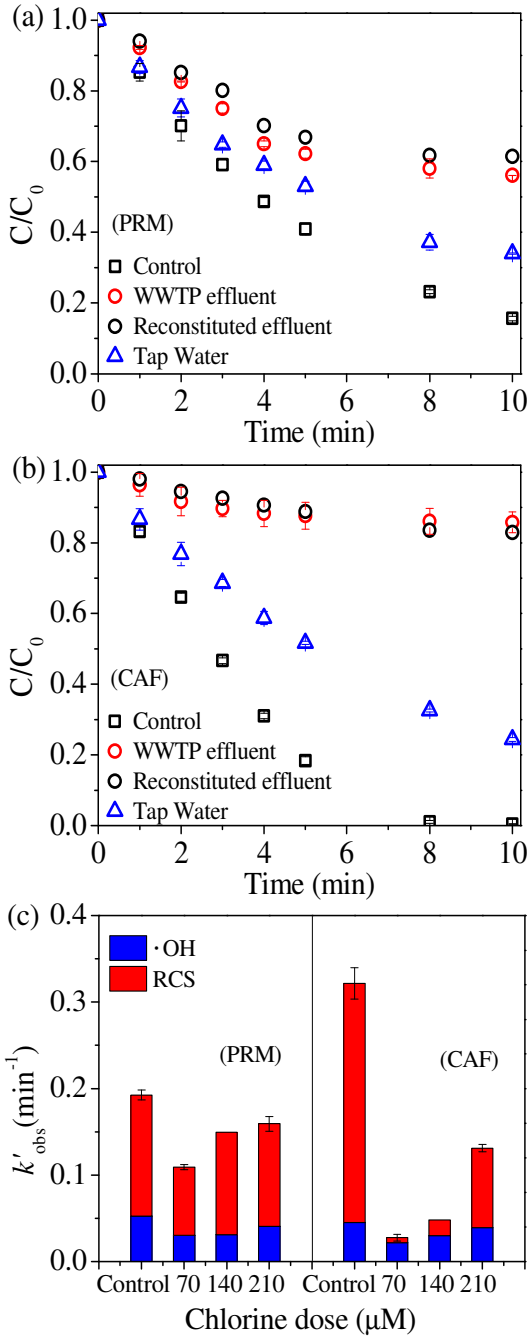

Figure 7. Decay of (a) PRM and (b) CAF in WWTP effluent, reconstituted effluent, and tap water in the UV/chlorine (70 μM) process; (c) k'_{obs} of PRM and CAF at different chlorine dose in WWTP effluent using 1μM NB as radical probe. Conditions: [PRM] = [CAF] = 5 μM, pH=7.76 for WWTP and reconstituted effluent, pH = 7.21 for tap water.

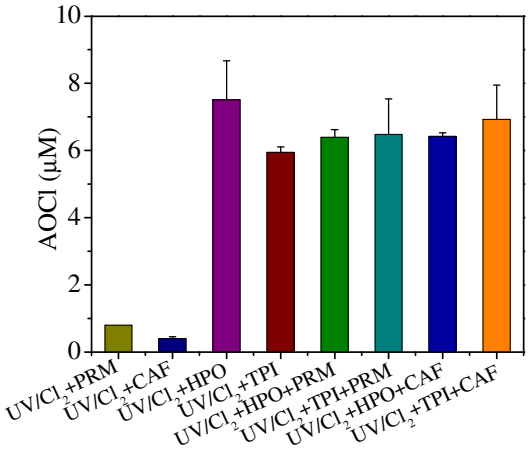

Figure 8. Formation of AOCl under different conditions. Conditions: [PRM] = [CAF] = 5 μM, [HPO] = [TPI] = 5 mg-C L^{-1}, [chlorine] = 70 μM, pH = 7.

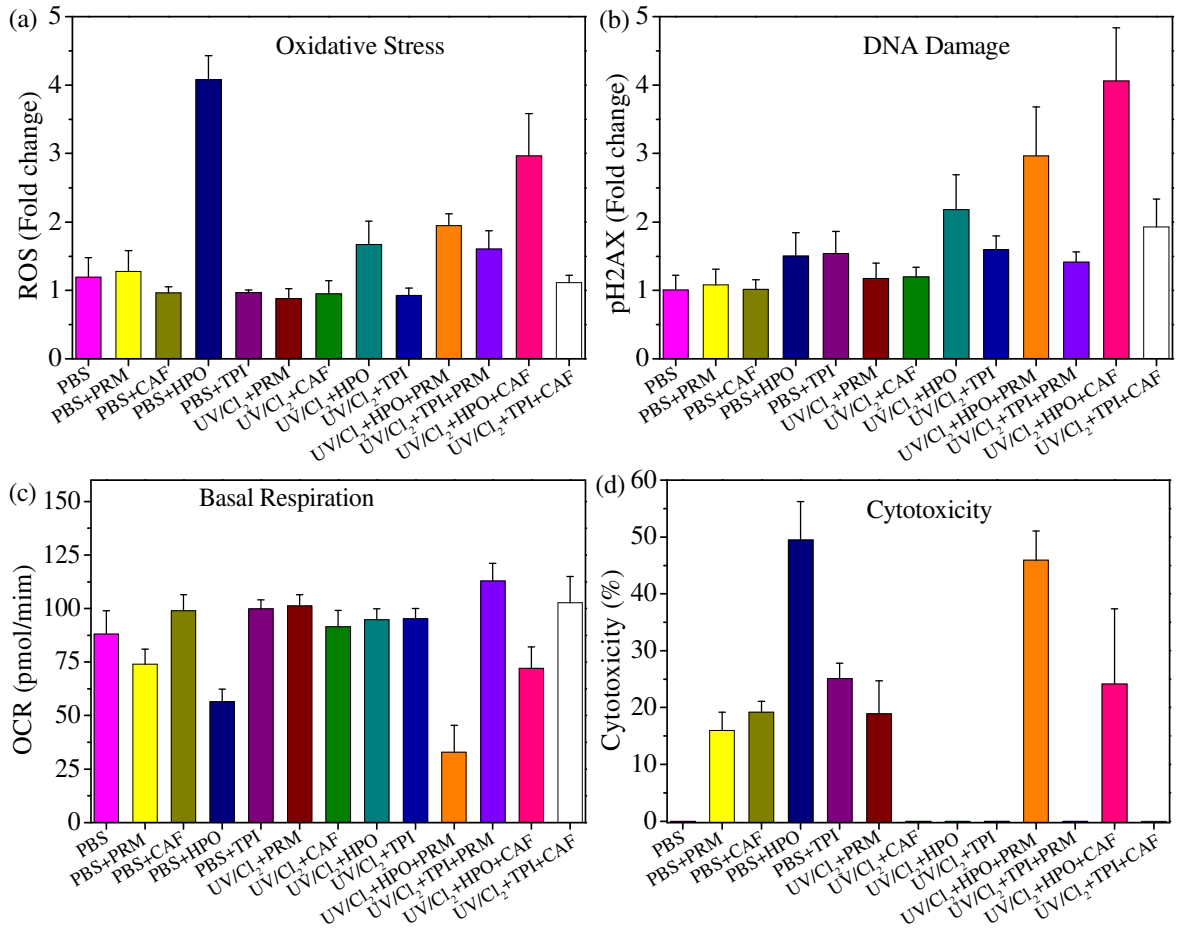

Figure 9. Impact of EfOM isolates on the oxidative stress, DNA damage, basal respiration, and cytotoxicity of UV/chlorine treatment of PPCPs. Conditions: [PRM] = [CAF] = 5 μM, [HPO] = [TPI] = 5 mg-C L^{-1}, [chlorine] = 70 μM, pH = 7.

Graphical abstract: